Progress In Electromagnetics Research C, Vol. 120, 119–133, 2022

A Novel Antipodal Vivaldi Antenna with Quad Band Notch Characteristics for UWB Applications

Vikas K. Rai[1, *], Mithilesh Kumar[1], and Shyama P. Chakraborty[2]

Abstract—This work presents a design and analysis of a high gain Antipodal Vivaldi Antenna (AVA) with quad band notch characteristics for Ultra-Wideband (UWB) applications. The proposed AVA is designed on a 1.2 mm FR4 substrate with dielectric constant 4.3 and loss tangent 0.025. Initially, the AVA parameters are optimized in a full wave simulator to get the required UWB performance. The UWB performance is further improved significantly by cutting a C-shaped slot from the AVA flares. The C-shaped slot introduces an extra resonance that widens the initial bandwidth. The band-notched filtering characteristics are achieved by — adding a Sun Shaped Slot (SSS) on the top and bottom flares of the AVA, inserting a hexagonal shaped Complimentary Split Ring Resonator (CSRR) on the ground plane of the AVA, and finally by inserting vias on either side of the feed line. The first designed notch band is from 2.2–2.7 GHz, covering the Bluetooth region. The second notch band is designed from 3.3–3.6 GHz, corresponding to WiMAX applications, and the third notch band is from 4.6–5.7 GHz corresponding to the WLAN band. Finally, a notch is fashioned from 8.8–9.5 GHz, corresponding to ITU applications. The simulated and measured return loss plots show that the antenna achieves an impedance bandwidth of 1.15–14 GHz with a reflection coefficient less than −10 dB, except at the four eliminating bands. To the best of the authors knowledge, the proposed technique is novel, and it allows good narrowband rejection over the UWB regime.

1. INTRODUCTION

The research on Ultra-Wideband (UWB) has become a booming topic from the moment Federal Communications Commission (FCC) approved the usage of the band from 3.1 to 10.6 GHz for the commercial use of UWB communication in 2002 [1]. It is necessary to eliminate the frequency interference between UWB systems and several other narrow band systems coexisting with the UWB systems such as the Worldwide Interoperability for Microwave Access (WiMAX), Bluetooth and Wireless Local Area Network (WLAN) bands. An effective method to overcome the above challenges is to develop a wideband UWB antenna with different notch bands to eliminate frequency interferences between different bands.

Different antennas with band-notched characteristics are extensively searched and reported in [2–9]. Planar monopole antennas [2], frequency-independent antennas [3, 4], and tapered slot antennas [5] are widely used in UWB systems. Most of these antennas have the same performance characteristics such as low profile, easy-to-manufacture, easy integration, and light weight. In addition, Vivaldi antenna [5–7], which is also called as tapered slot antenna, is a good candidate for UWB applications. Vivaldi aerial was developed by Gibson in 1979 and later modified by Gazit to form the Antipodal Vivaldi Antenna (AVA). The microstrip to double slot line transition brings about good impedance matching in a Vivaldi aerial. In comparison with the omnidirectional radiation patterns of planar monopole antenna, AVA

Received 24 February 2022, Accepted 7 May 2022, Scheduled 10 May 2022
* Corresponding author: Vikas Kumar Rai (hellovikasrai@yahoo.com).
[1] Department of Electronics Engineering, Rajasthan Technical University, Kota, Rajasthan 324010, India. [2] CARE, Indian Institute of Technology Delhi, Hauz Khas, New Delhi 110016, India.

has a highly directional radiation pattern. Many papers investigate and introduce the function of AVA and its performance enhancement characteristics in [8, 9].

Introducing three resonators to create triple band-notched characteristics in an antipodal structure is elaborately discussed in [10]. A generalized method to introduce a notch in any planar antenna including etching slots and slits on the ground plane or on the radiator is reported in [11–14]. Another technique to introduce notch characteristics is to add resonators on the radiation element or near the feed-lines as clearly discussed in [15–18]. A U-shaped slot [19], an X-shaped slot [20], capacitive loaded loop (CLL) resonators [21], and stepped-impedance resonator (SIR) [22, 23] are inserted in an UWB AVA to notch out various narrowband frequencies.

In this work, an AVA with quad band-notched characteristics is implemented for UWB applications. A conventional AVA is designed first followed by the introduction of various modifications to achieve different narrow band rejections at different frequencies. The bandwidth of the CAVA is improved first to extend the operating region of the AVA by adding a C-shaped slot. The first notch band is obtained from 2.2–2.7 GHz with a Sun Shaped Slot (SSS). Two different notches are obtained, one operating from 4.6–5.7 GHz and the other from 8.8–9.5 GHz by loading a hexagonal shaped Split Ring Resonator (SRR) on the ground plane. The final notch is achieved from 3.3–3.6 GHz by loading vias close to the feed structure.

2. PROPOSED ANTENNA GEOMETRY AND DESCRIPTION

The various dimensions of the proposed AVA are calculated using Equations (1) to (5).

Length (L) of the Vivaldi antenna should be greater than half of the wavelength (λ),

$$L > \frac{\lambda}{2} \tag{1}$$

where λ is the maximum operating wavelength.

Width (W) of the Vivaldi antenna should be greater than one-fourth of the wavelength (λ),

$$W > \frac{\lambda}{4} \tag{2}$$

The equation of outer tapering edge is given by,

$$x_1 = A_1 \left(e^{y r_1^{n1}} - 1 \right) - \frac{1}{2} TW \tag{3}$$

The equation of inner tapering edge is given by,

$$x_2 = A_2 \left(e^{y r_2^{n2}} - 1 \right) + \frac{1}{2} TW \tag{4}$$

The taper rates are given by,

$$r_1 = \left\{ \frac{\log\left(\frac{w_1/2 + A_1 - TW/2}{A_1}\right)}{H} \right\}^{\frac{1}{n1}} \quad r_2 = \left\{ \frac{\log\left(\frac{w/2 + A_2 - TW/2}{A_2}\right)}{H_1} \right\}^{\frac{1}{n2}} \tag{5}$$

Figure 1(a) corresponds to the layout of the designed CAVA with dimensions of $123.9 \times 105.2\,\text{mm}^2$ on an FR4 substrate with a dielectric constant of 4.3, thickness of 1.2 mm, and loss tangent ($\tan\delta$) of 0.025. Copper with conductivity $\sigma = 5.8 \times 10^7\,\text{S/m}$ is used as conducting material on the top and bottom of the substrate with a thickness of $t = 0.035\,\text{mm}$. Microstrip line feeding technique is used to excite the designed antenna. The width and length of the proposed antenna are denoted by W and L, the exponential taper profile amplitudes denoted by A_1 and A_2, the opening of the flares denoted W_1, the taper length represented by TL or H, and the inner profile height denoted by H_1. The exponent terms n_1 and n_2 are taken as 2 and 5, respectively. The feed line width TW is chosen such that the input impedance of the antenna is $50\,\Omega$. The mouth opening or taper width (W_1) is chosen to be greater than $\frac{\lambda_{\max}}{2}$, with $\lambda_{\max}$ being the free space wavelength corresponding to the lowest frequency of operation (1.7 GHz). To improve the return loss and improve the impedance matching, the feed design on the

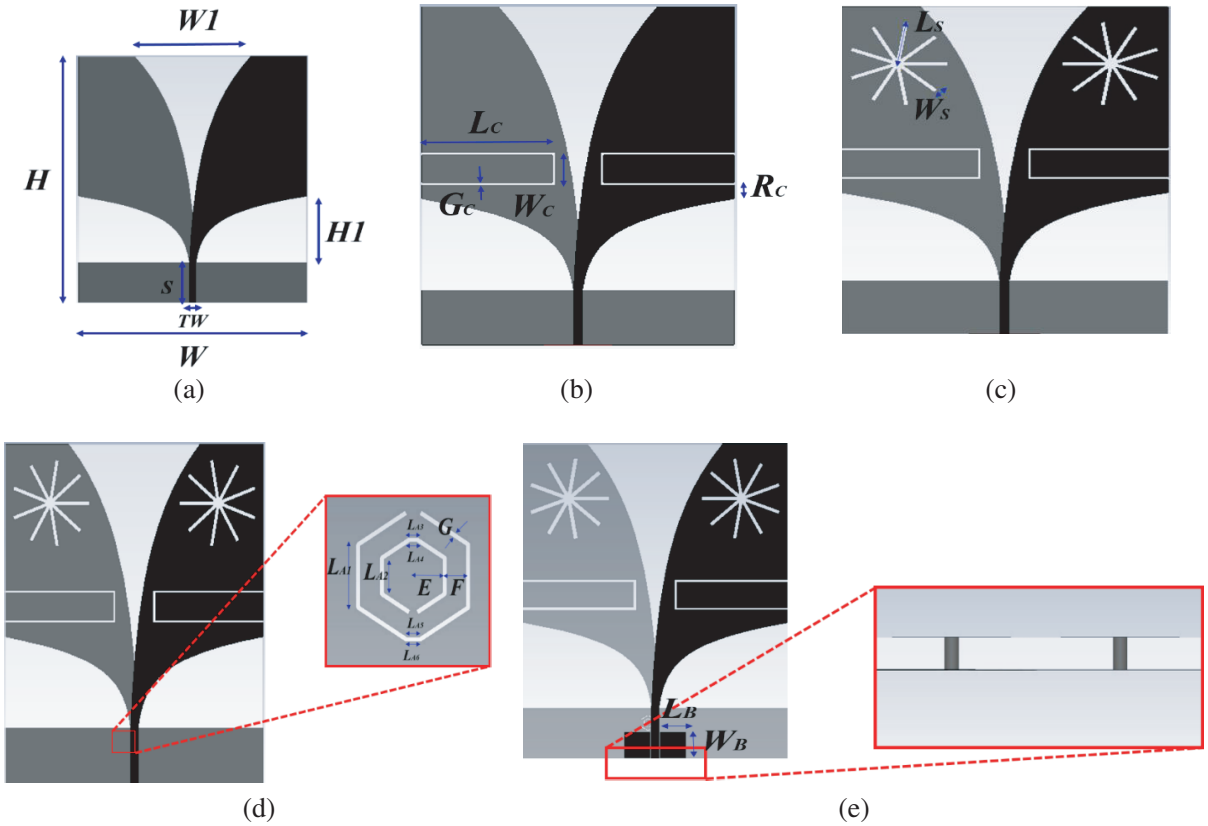

Figure 1. The design stages in the development of the proposed quad band notch antenna. (a) Stage 1, (b) Stage 2, (c) Stage 3, (d) Stage 4 and (e) Stage 5.

ground plane is modified by introducing a rectangle-shaped strip as a ground plane on the back side of the antenna. The dimension of the rectangular strip is given by $W \times S$. The antenna designed up to this stage has been designated as Stage 1. In the later stages, the lower cutoff frequency of 1.7 GHz is obtained based on the aperture width in between the flares, denoted by W_1. A C-shaped slot of dimensions $L_C \times W_C$, with a thickness of G_C, is etched out from the flares on both the top and bottom of the flares, as depicted in Fig. 1(b). This modification further extends the lower cutoff frequency of the proposed antenna. The major contribution of this work is to design four notch bands in the UWB frequency range to avoid interferences between various systems operating in the UWB range with other systems operating in the Bluetooth, WLAN, WiMAX, and ITU ranges. A sun-shaped slot on the flares is designed on the top and bottom of the flares, as depicted in Fig. 1(c). Initially, a slot of dimension $L_S \times W_S$ is designed in the simulator. The designed slot is rotated by 40° clockwise, and nine copies are made to form an SSS. A similar SSS is made on the ground flare. The SSS introduces a notch from 2.2–2.7 GHz, corresponding to the Bluetooth band. A hexagon-shaped SRR is introduced in the ground plane to achieve two notches corresponding to WLAN and ITU bands, operating from 4.6–5.7 GHz and 8.8–9.5 GHz, respectively. Finally, two square parasitic patches with vias are introduced near the antenna feed to introduce the last notch from 3.3–3.6 GHz for WiMAX applications. All the optimized parameters are listed in Table 1.

3. SIMULATED RESULTS AND DISCUSSION

The proposed antenna is designed and simulated using commercially available Computer Simulation Technology (CST) Microwave Studio 2016. The proposed antenna is fed using a waveguide port in the simulator. The simulated return loss plot obtained at different design stages leading up to the final structure is depicted in Fig. 2(a). The final return loss plot with the quad band notches separately

Table 1. Geometrical parameters of the proposed notch-band antenna.

L	W	A_1	A_2	r_1	r_2	n_1	n_2
123.9	105.2	1.6	1.2	0.167	0.645	2	5
H	TW	S	W_1	H_1	L_C	G_C	W_C
123.9	2.9	20	53.58	53.58	45	1	12
R_C	L_S	W_S	L_{A1}	L_{A2}	L_{A3}	L_{A4}	L_{A5}
5	16	1.5	2.8	1.6	0.53	0.33	0.65
L_{A6}	E	F	G	L_B	W_B	R	h
0.85	1.6	1.2	0.2	10	10	0.6	1.2

All dimensions are in mm

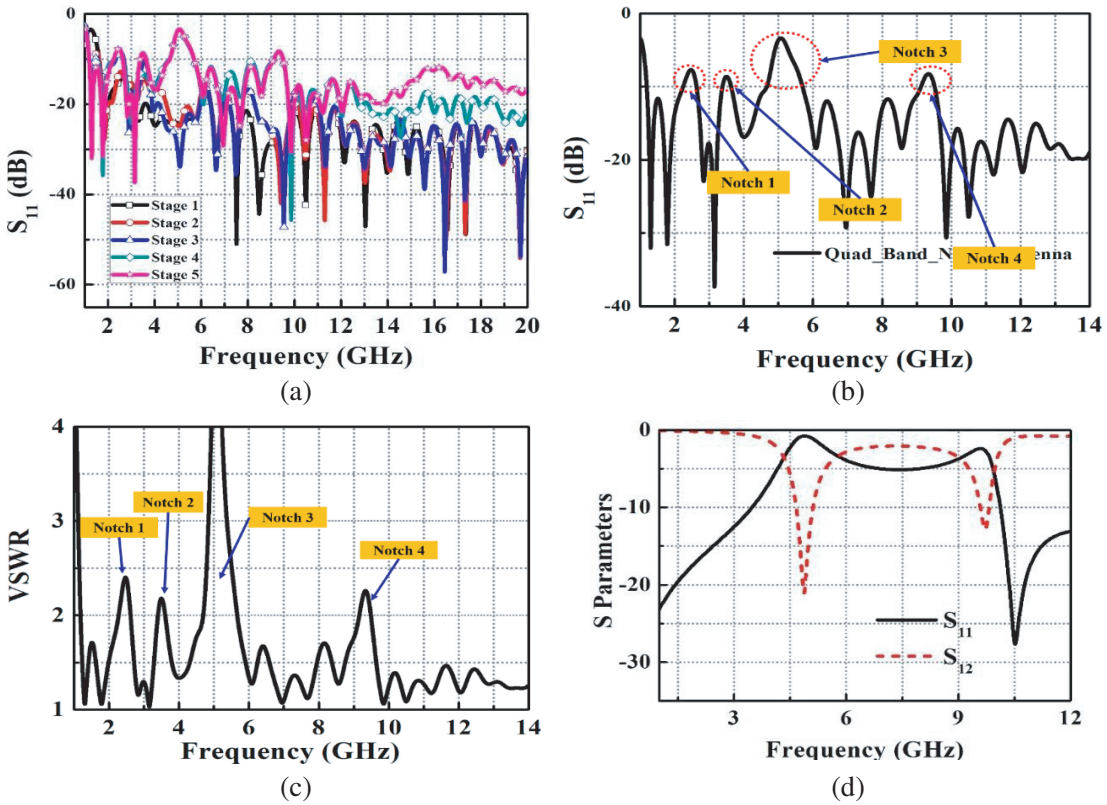

Figure 2. Simulated (a) return loss at different stages, (b) return loss plot with quad band notch characteristics, and (c) VSWR responses of the proposed antenna, (d) simulated S-Parameters of the designed Hexagonal shaped CSRR.

labelled is displayed in Fig. 2(b). The simulated VSWR plot of the proposed design is also observed and the response is depicted in Fig. 2(c). Fig. 2(d) displays the S-parameters of the designed CSRR. The stopbands can be observed from 4.5–5.8 GHz and from 8.9–9.6 GHz, corresponding to the obtained notch bands. The real and imaginary parts of the relative permittivity is shown in Fig. 3(a). The imaginary part of γ_r is negative from 4.8–9.9 GHz. Finally, the relative permeability values are shown in Fig. 3(b) where imaginary part of it is negative from 2.8–4.8 GHz.

The equivalent circuit of the proposed structure is displayed in Fig. 4(a). In this structure, via is modelled as a parallel RLC circuit that is responsible for the notch band from 3.3–3.6 GHz. This is

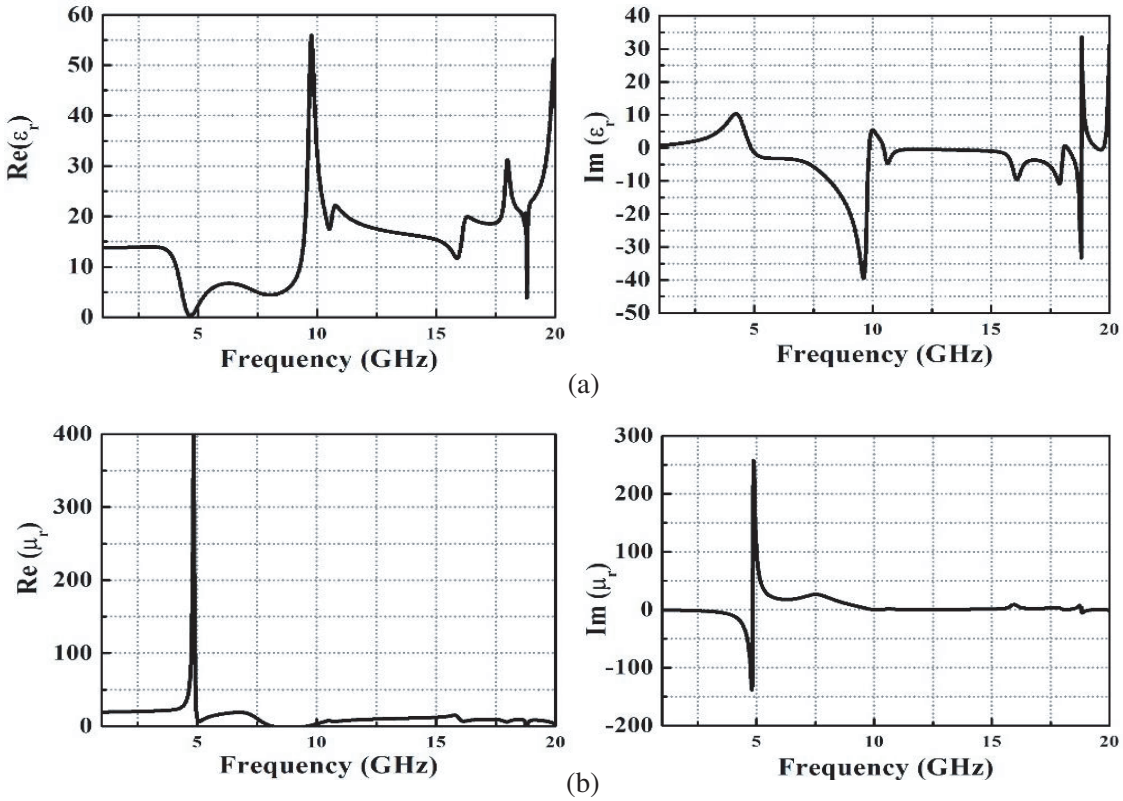

Figure 3. Real and imaginary values of the (a) ε_r, and (b) μ_r.

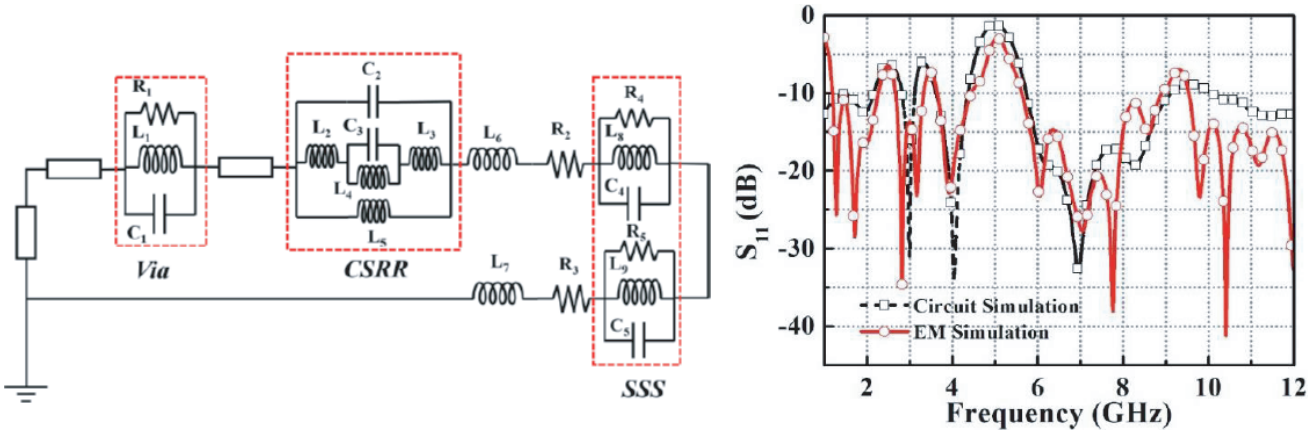

Figure 4. (a) Equivalent circuit model of the proposed quad band notch antenna. (b) Comparison of matching with the circuit model versus EM simulation.

followed by the addition of a second order LC circuit to incorporate the notch bands from 4.6–5.7 GHz and 8.8–9.5 GHz. The SSS on the flare edge of the AVA is modelled as a parallel RLC circuit. All the lumped components are tuned to a reasonable extent in Keysight Advanced Design Systems (ADS) circuit simulator. Table 2 gives the optimized parameters of the final equivalent circuit model. The obtained EM simulation results and tuned circuit simulation results are compared and displayed in Fig. 4(b). Note that the circuit simulation results closely match the EM simulation results.

The proposed antenna has a directional radiation pattern in the E plane as well as in the H

Table 2. Optimized lumped component values of the equivalent circuit model.

R_1	R_2	R_3	R_4	R_5
83.75 Ω	23.154 Ω	23.154 Ω	300 Ω	300 Ω
C_1	C_2	C_3	C_4	C_5
4.5 pF	1.645 pF	0.75 pF	3.5 pF	3.5 pF
L_1	L_2	L_3	L_4	L_5
0.75 nH	0.15 nH	0.15 nH	0.265 nH	29 nH
L_6	L_7	L_8	L_9	
0.5 nH	0.5 nH	0.8 nH	0.8 nH	

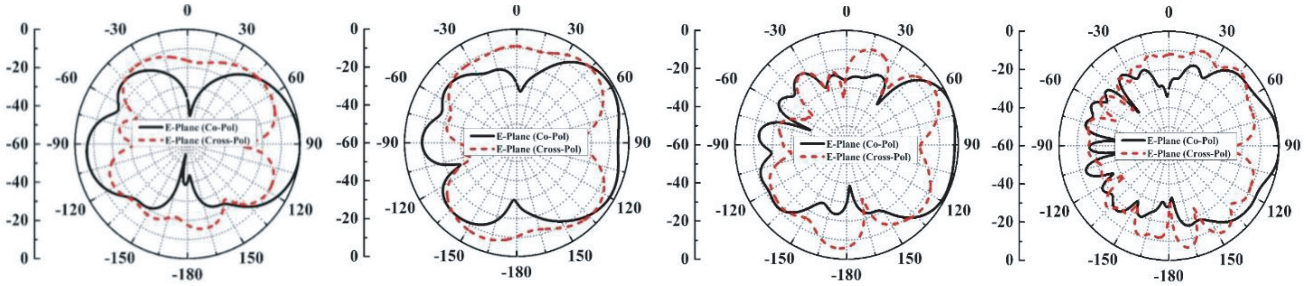

Figure 5. The simulated E plane radiation pattern of the proposed antenna at various notch band frequencies. (a) 2.5 GHz, (b) 3.5 GHz, (c) 5.2 GHz and (d) 9.3 GHz.

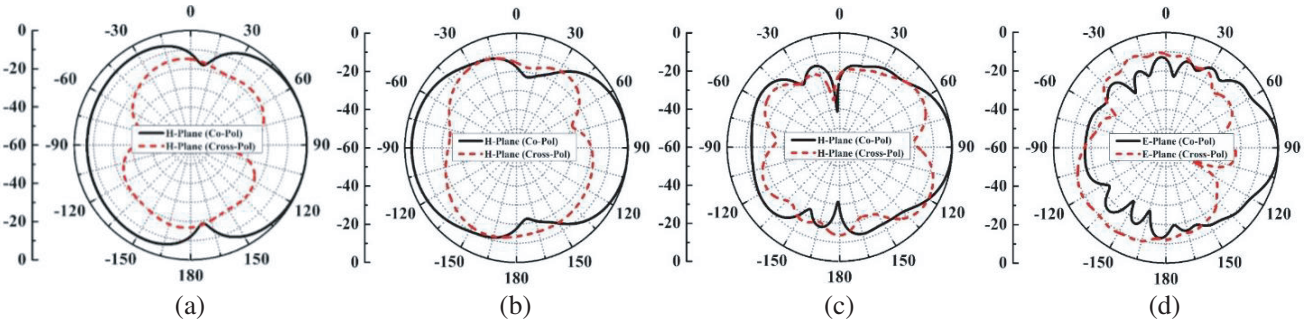

Figure 6. The simulated H plane radiation pattern of the proposed antenna at various notch band frequencies. (a) 2.5 GHz, (b) 3.5 GHz, (c) 5.2 GHz and (d) 9.3 GHz.

plane. E- and H-plane radiation patterns of the proposed antenna at 2.5 GHz, 3.5 GHz, 5.2 GHz, and 9.3 GHz, with each frequency corresponding to a particular notch band are depicted in Fig. 5 and Fig. 6, respectively. The frequencies outside the notch characteristics are noted, and the radiation patterns are also plotted. Fig. 7 and Fig. 8 depict the E- and H-plane radiation patterns at 3 GHz, 4 GHz, 6 GHz, and 8 GHz, respectively. Clear pattern distortion appears in Fig. 5 and Fig. 6 as they display the antenna radiation patterns within the notch band.

Figure 9(a) presents the gain variation of the notch-band antenna at the different stages. The gain decays at the positions of the band notches. Peak gains at the four notch frequencies bands are listed in Table 3. Simulated radiation efficiency responses are shown in Fig. 9(b). Fig. 10(a) depicts the surface current distribution at 2.5 GHz. It can be observed that the currents are concentrated near the SSS, and it also validates the notch band at 2.2–2.7 GHz. Fig. 10(b) depicts the current concentration on the two patches introduced near the microstrip feed line at 3.5 GHz. It clarifies the second notch band from

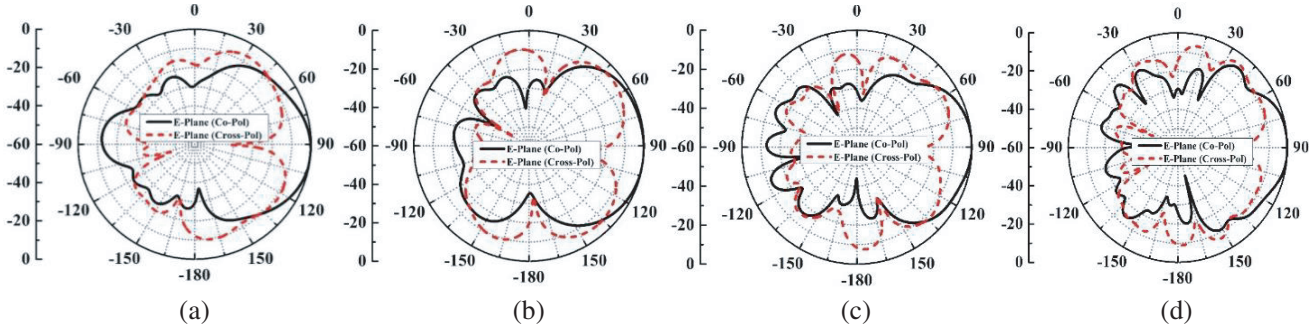

Figure 7. The simulated E plane radiation pattern of the proposed antenna at various frequencies outside the notch band. (a) 3 GHz, (b) 4 GHz, (c) 6 GHz and (d) 8 GHz.

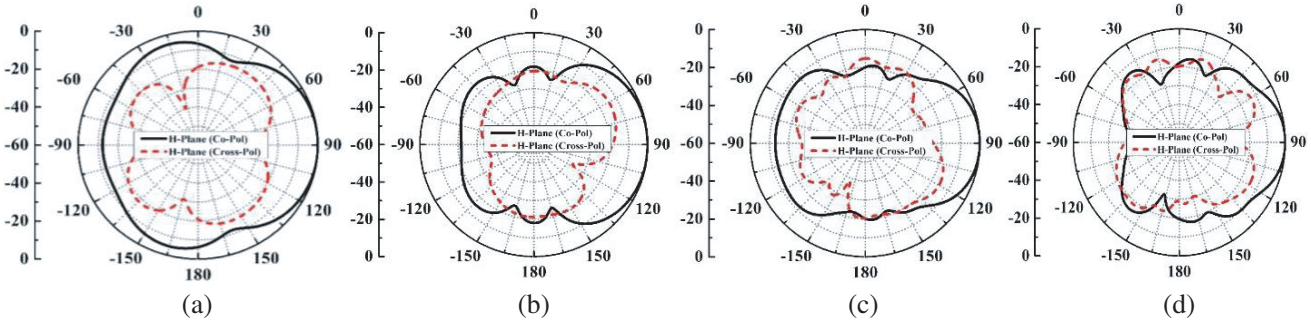

Figure 8. The simulated E plane radiation pattern of the proposed antenna at various frequencies outside the notch band. (a) 3 GHz, (b) 4 GHz, (c) 6 GHz and (d) 8 GHz.

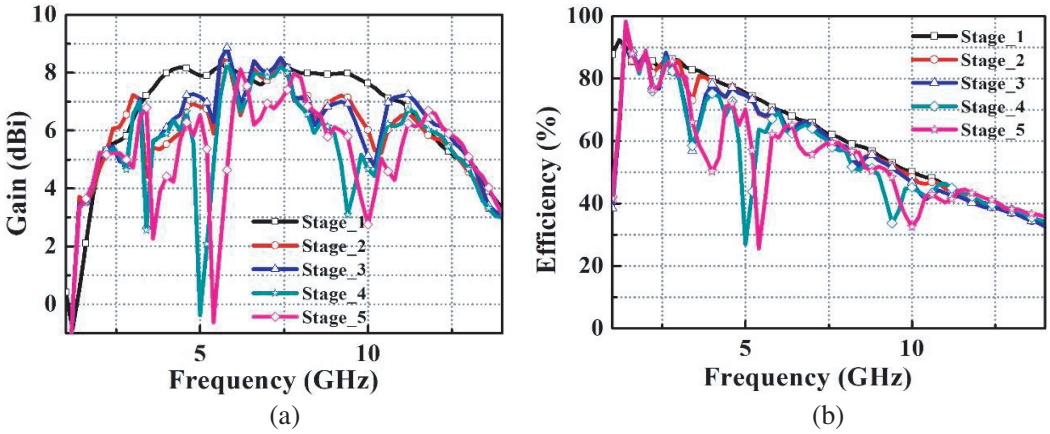

Figure 9. Simulated (a) gain and (b) efficiency versus frequency at different stages of the antenna.

3.3–3.6 GHz by the parasitic patch along with the vias connecting the patch to the ground plane. In Figs. 10(c)–(d), the current density is the highest on the hexagonal CSRR. It confirms the notch bands at 4.6–5.7 GHz and 8.8–9.5 GHz bands.

In order to perform the time domain analysis, a similar copy of the proposed antenna is designed and placed at a distance greater than the far field distance (200 mm), as shown in Fig. 11(a). A Gaussian pulse is used as the excitation signal, and it is depicted in Fig. 11(b). This is the default signal in CST Microwave Studio. The obtained time domain signal is shown in Fig. 11(c). Group delay measures the amount of distortion produced by the signal radiated from the antenna up to a distance. The simulated group delay of the antenna is shown in Fig. 11(d). Result shows a flat phase response. The antenna

Table 3. Simulated peak gains at specific frequencies in the notch band.

Notch 1	Notch 2	Notch 3	Notch 4
2.2–2.7 GHz	3.3–3.6 GHz	4.6–5.7 GHz	8.8–9.5 GHz
4.5 dB	2.7 dB	3.5 dB	3.5 dB

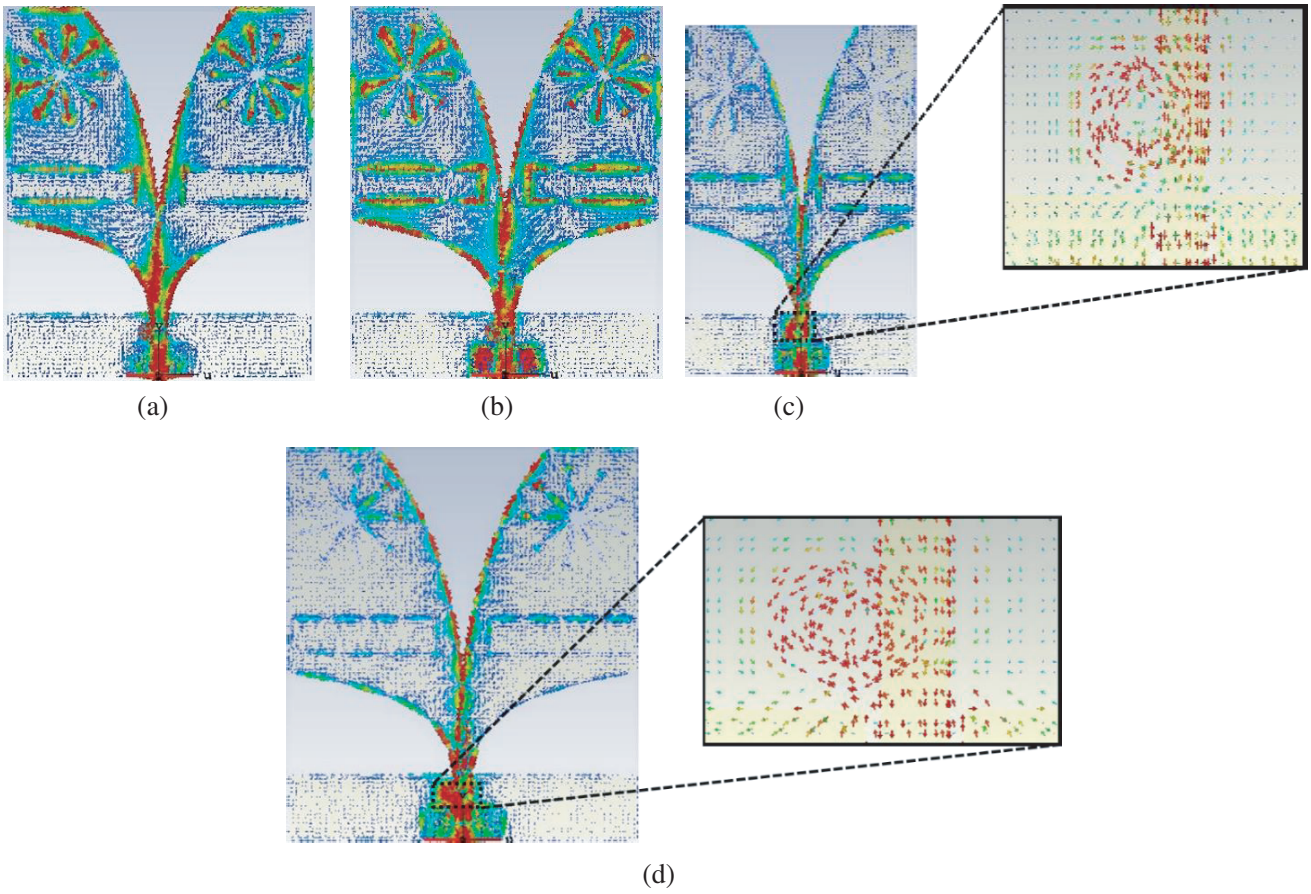

Figure 10. Surface current distribution of the proposed antenna at different notch band frequencies. (a) 2.5 GHz, (b) 3.5 GHz, (c) 5.2 GHz and (d) 9.3 GHz.

displays minimum phase distortion, except at the frequencies where the notches are present. Note that less distortion is produced between the transmitting and the receiving antennas in the passband region. The application of the proposed antenna is also tested for biomedical applications by finding out the Specific Absorption Rate (SAR) value at different frequencies outside the notch band. SAR is a measure of the amount of RF power deposited in the human head or body whenever a wireless radio device transmits. The frequencies outside the notch bands are considered as they have directional radiation pattern outside the notch band. The directional radiation helps in achieving good lateral resolution as well as good penetration at low frequencies. The SAR is calculated for testing the usability of the proposed antenna for breast tumor detection. It is calculated based on the expression, as given in (6)

$$\mathrm{SAR} = \sigma \frac{\left|E^2\right|}{\rho} \tag{6}$$

where σ is the conductivity (S/m) of the tissue, E the internal electric field (V/m), and ρ the mass

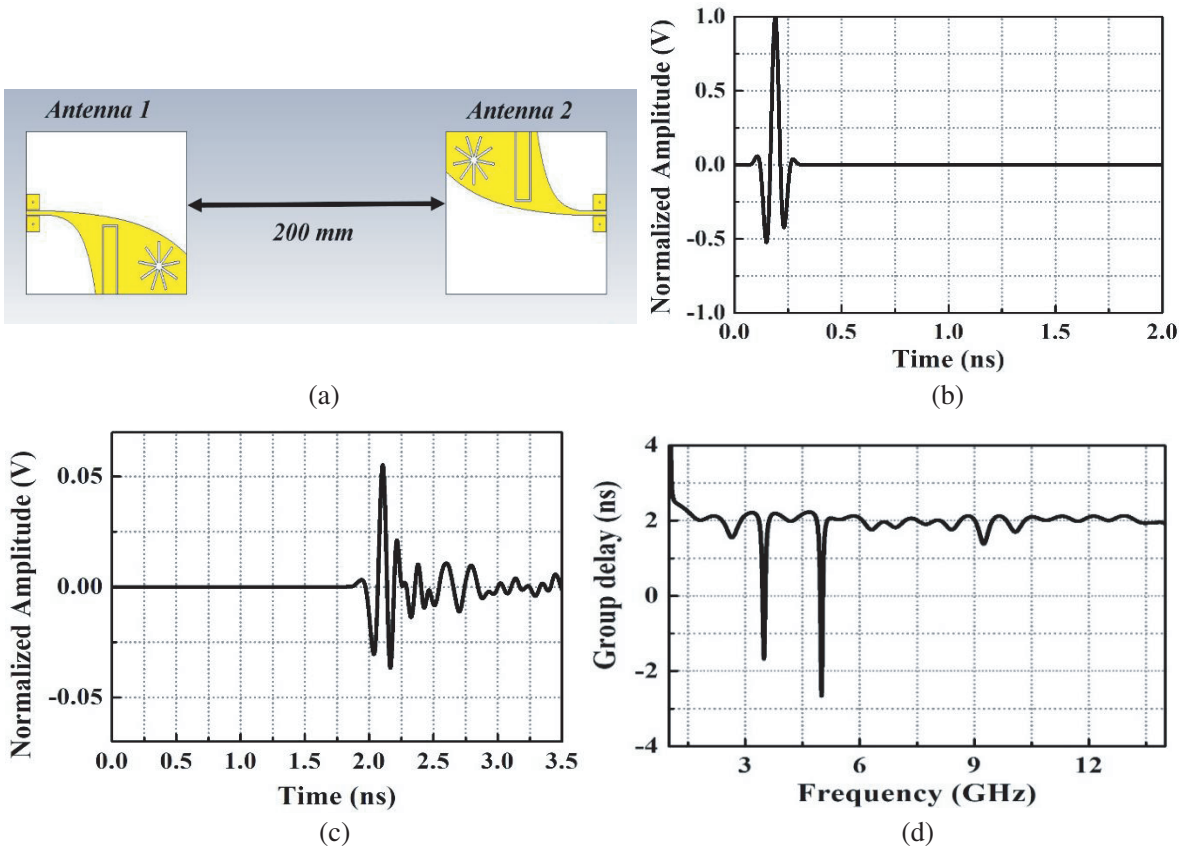

Figure 11. (a) Antenna setup to obtain the time domain responses in the simulator. (b) Normalized input and (c) output signals obtained by placing the antennas face to face. (d) Simulated group delay response of the proposed antenna.

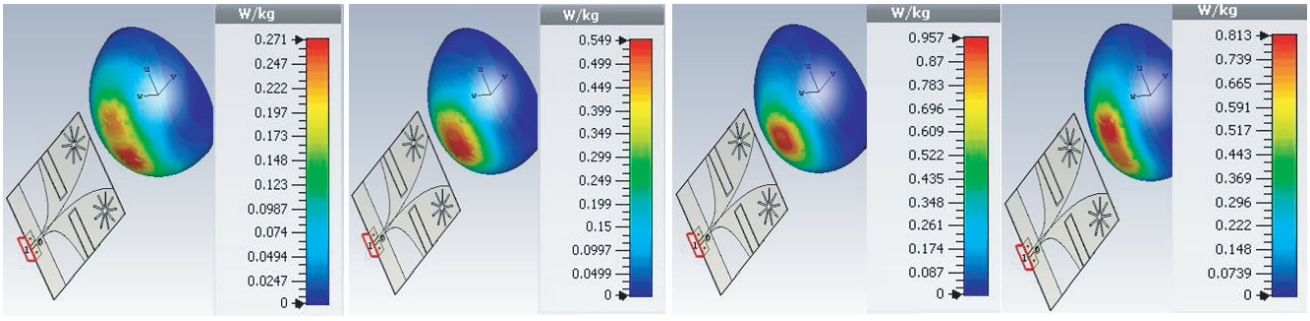

Figure 12. SAR verifications at (a) 3 GHz, (b) 4 GHz, (c) 6 GHz and (d) 8 GHz, with the antenna.

density (kg/m^3). The hemispherical breast phantom is made up of skin (Radius = 70 mm) and fat (*Radius* = 68 mm) layers, with a tumor (Radius = 5 mm) embedded in it at a depth of 25 mm from the skin layer. The phantom has been modelled with the CST Microwave studio library. The SAR values at 3 GHz, 4 GHz, 6 GHz, and 8 GHz are obtained and depicted clearly in Figs. 12(a)–(d), respectively. The SAR values obtained in all the cases are less than 1.6 W/kg, which shows that the proposed antenna can also be utilized for imaging applications.

4. EXPERIMENTAL RESULTS AND DISCUSSION

The prototype of the quad band notch antenna is fabricated on an FR-4 substrate with a size of $123.9 \times 105.2\,\text{mm}^2$ and thickness of 1.2 mm. Fabricated images of the front and back sides of the antenna are shown in Figs. 13(a)–(b). Fig. 13(c) shows measurement setup inside an anechoic chamber. S-parameter of the antenna is tested using the N5224B vector network analyzer (VNA) from Keysight. Measured S_{11} response of the antenna is shown in Fig. 13(d). Result shows that the measured S_{11} variation closely follows the simulated response. Measured and simulated impedance bandwidths are documented in Table 4 for better clarity. Note that discrepancies between simulated and measured notch bands are negligible. It is mostly attributed to the fabrication error, losses from the soldering the SMA connector, and via loaded parasitic patch.

Radiation patterns of the antenna are tested inside the anechoic chamber where the proposed antenna is placed at the receiving end. The distance between transmitting horn and the proposed antenna is fixed at 1 meter which satisfies the far-field condition. The power to the transmitting horn antenna is 10 dBm. Fig. 14 and Fig. 15 present measured E- and H-plane radiation patterns

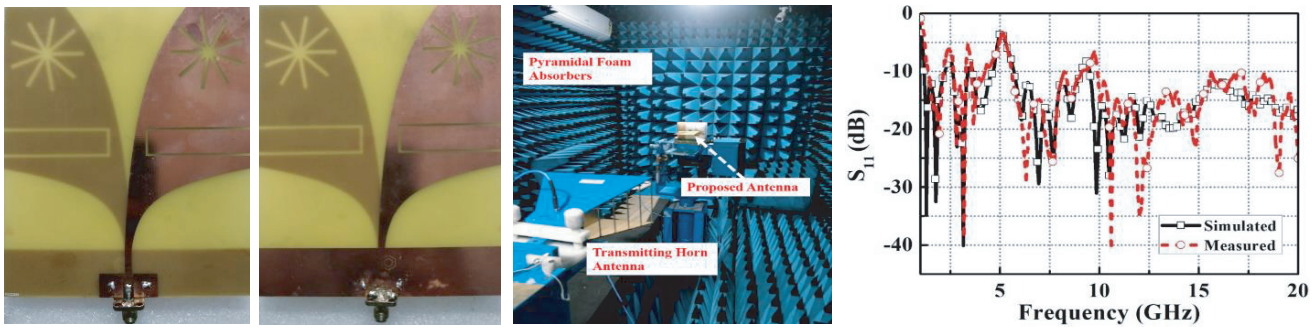

Figure 13. Fabricated (a) front and (b) back side images of the proposed antenna. (c) Measurement set up inside the anechoic chamber. (d) Measured versus simulated reflection coefficient responses.

Table 4. Measured and simulated notch bandwidth for the proposed antenna.

Notch bandwidth for $S_{11} > -10$ dB							
1st notch band		2nd notch band		3rd notch band		4th notch band	
Simulated	Measured	Simulated	Measured	Simulated	Measured	Simulated	Measured
2.2–2.7 GHz	2.15–2.7 GHz	3.3–3.6 GHz	3.25–3.58 GHz	4.6–5.7 GHz	4.4–5.64 GHz	8.8–9.5 GHz	8.8–9.8 GHz

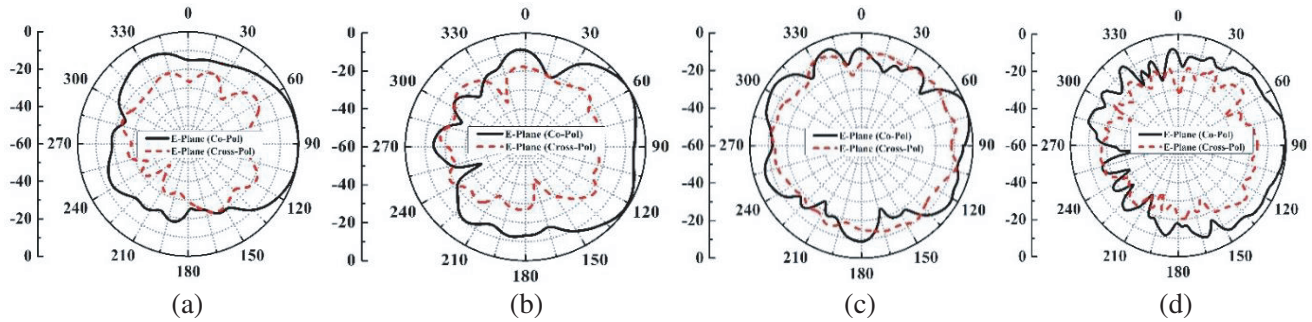

Figure 14. The measured E plane radiation pattern of the proposed antenna at various notch band frequencies. (a) 2.5 GHz, (b) 3.5 GHz, (c) 5.2 GHz and (d) 9.3 GHz.

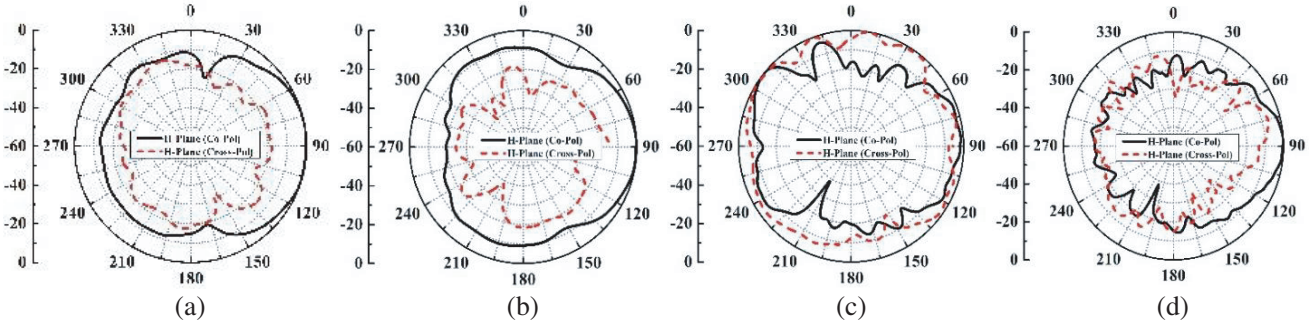

Figure 15. The measured H plane radiation pattern of the proposed antenna at various notch band frequencies. (a) 2.5 GHz, (b) 3.5 GHz, (c) 5.2 GHz and (d) 9.3 GHz.

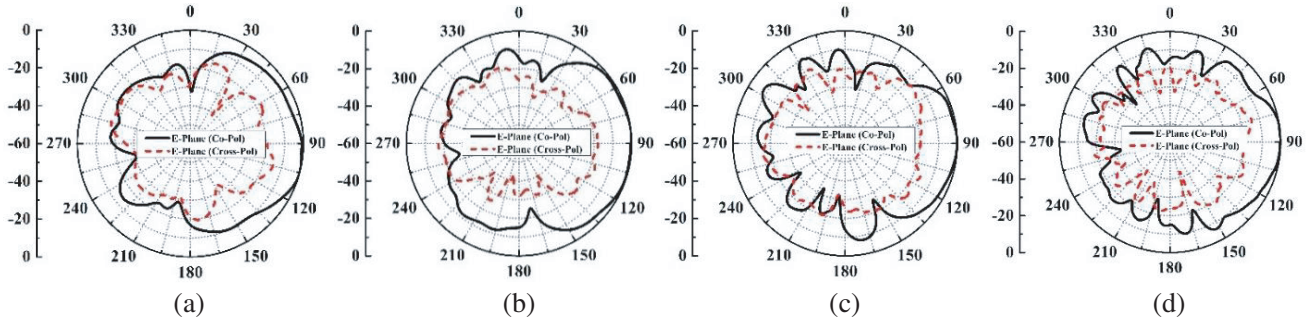

Figure 16. The simulated E plane radiation pattern of the proposed antenna at various frequencies outside the notch band. (a) 3 GHz, (b) 4 GHz, (c) 6 GHz and (d) 8 GHz.

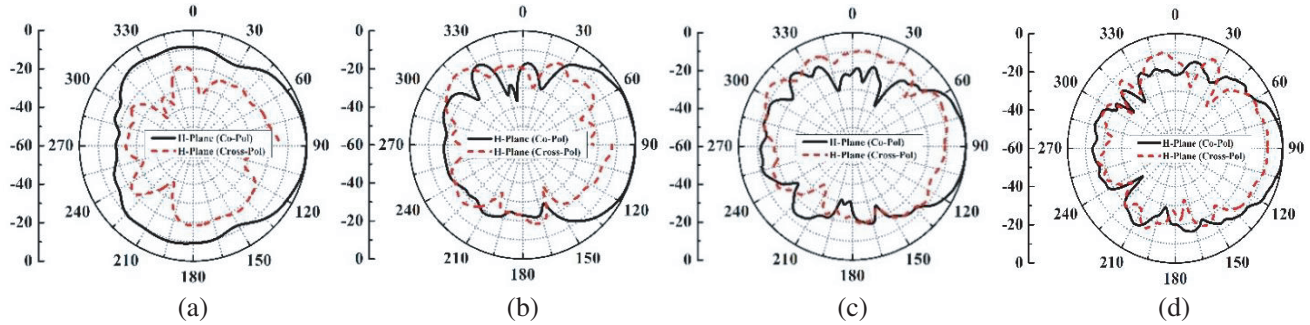

Figure 17. The simulated H plane radiation pattern of the proposed antenna at various frequencies outside the notch band. (a) 3 GHz, (b) 4 GHz, (c) 6 GHz and (d) 8 GHz.

at 2.5 GHz, 3.5 GHz, 5.2 GHz, and 9.3 GHz, respectively. The E- and H-plane radiation patterns at different frequencies (3 GHz, 4 GHz, 6 GHz, and 8 GHz) outside the notch band are plotted in Fig. 16 and Fig. 17, respectively, for better clarity. It can be observed that the proposed antenna maintains its directive radiation with no pattern distortion at all these frequencies outside the notch band. However, clear pattern distortion is obtained at frequencies within the band reject band.

The gain of the antenna in the UWB is determined using the gain transfer method. The gain of the standard gain horn (SGH) antenna is noted from the datasheet. Tx horn is connected to a VNA with 5.5 m long cable, and the antenna is connected with a coaxial cable to port 2 of the VNA. The received power is recorded from the VNA. The power is found at frequencies from 1 to 14 GHz. Initially, the designed antenna is replaced with SGH, and the received power is noted at the frequencies from 1 to 14 GHz. This is termed as P_{SGH}. By keeping the transmitting power and the distance between transmitter and receiver antennas unchanged, SGH at the receiver end is replaced with the proposed

Table 5. Performance comparison table with other similar categories.

References	Antenna Size (mm^2)	Bandwidth (GHz)	Peak Gain (dBi)	Rejected Band	No. of Rejected Bands	Techniques Utilized to implement notch
[25]	66.3 × 66.3	3–11	Around 11	3.6–3.9, 5.6–5.8	2	Compact EBG Structures
[26]	90 × 60	UWB	8.04	3.21–3.8, 5.12–5.80	2	Mushroom Type EBG Structure
[27]	45 × 40	0.45–12	5.5	0.45–0.85, 5.1–5.8, 3.3–3.8	3	Meander line, Pin diode
[28]	30 × 40	3.10–10.60	Around 4.2	3.4–3.7, 5.15 -5.35, 5.72–5.82	3	Radiation patch connected through a via with the strip placed beneath the patch
[29]	38.5 × 38.5	3.08–10.80	Around 3.6	5.03–5.97	1	L shaped slits on the ground plane
[30]	36 × 36	3.10–10.60	Around 6.8	5.15–5.825	1	Introducing slits in the radiator
[31]	48 × 48	2.50–12.00	Around 6	5.1–6	**1**	Introduction of SRR on the radiator
[32]	22 × 36	3.10–11.0	5	5.15–5.85	**1**	Introduction of a strip in the ground plane
[33]	26 × 28	2.70–10.90	1.6–6.2	5.1–5.9, 6.7–7.1	**2**	Two SRRs on the ground plane
[34]	37 × 46	2.5–12	4	3.5–3.9 5.6–6.2	**2**	Square Ring and C shaped slot
[35]	11.5 × 14.5	2.2–14	Around 4	3.4–3.7 5.2–5.8	**2**	T shaped slit and C shaped parasitic elements
Proposed Work	123.9 × 105.2	**1.1–14**	**8.15**	**2.2–2.7, 3.3–3.6, 4.7–5.6, 8.8–9.5**	**4**	**Sun Shaped Slot, Hexagonal SRR, Metallic Patch with via**

antenna, and the received power is noted at those frequencies. It is denoted as P_{AUT}. Then the antenna gain is obtained using Eq. (7) [24].

$$(GAUT)\,\mathrm{dB} = (GSGH)\,\mathrm{dB} + 10\log 10\left(\frac{PAUT}{PSGH}\right) \tag{7}$$

The measured gain of the proposed antenna is shown in Fig. 18. Result shows that the measured gain closely follows the simulated one in the entire frequency range of operation. Finally, Table 5 shows performances of the proposed antenna with other reported state-of-the-art antennas.

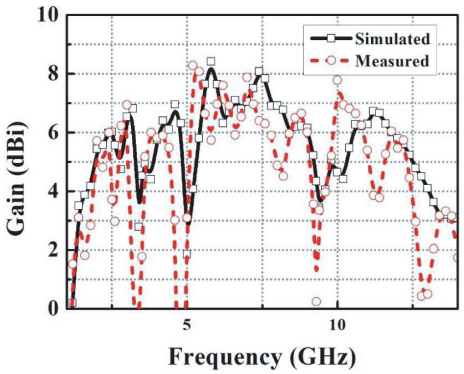

Figure 18. Measured versus simulated gain of the antenna.

5. CONCLUSION

In this work, the design and analysis of a high gain AVA with quad band notched characteristics for UWB applications is presented. The designed antenna has four notch characteristics at four different frequencies. The bandwidth of the designed CAVA is improved initially by the addition of a C-shaped slot. This is followed by the addition of an SSS to get the first notch from 2.2–2.7 GHz. A hexagon-shaped SRR is introduced with appropriate dimensions to induce two notch bands at 4.6–5.7 GHz and 8.8–9.5 GHz, respectively. Finally, two square patches with vias are introduced to get the last notch from 3.3–3.6 GHz. The return loss, gain, and radiation pattern of the proposed design are verified experimentally for all the cases. The good agreement between the simulated and measured results proves the utility of the proposed technique. In the opinion of authors, the proposed technique allows good narrowband rejection in the UWB region.

REFERENCES

1. Federal Communications Commission, "First Report and Order, Revision of Part 15 of the Commission's Rule Regarding Ultra-Wideband," 2002.
2. Ahmed, O. and A. R. Sebak, "A printed monopole antenna with two steps and a circular slot for UWB applications," *IEEE Antennas Wirel. Propag. Lett.*, Vol. 7, 411–413, 2008.
3. Dyson, J., "The equiangular spiral antenna," *IRE Trans. Antennas Propagat.*, Vol. 7, 181–187, 1959.
4. DuHamel, R. and D. Isbell, "Broadband logarithmically periodic antenna structures," *IRE Nat. Conv. Rec.*, 119–128, 1957.
5. Gibson, P. J., "The Vivaldi aerial," *Proc. 9th Eur. Microw. Conf.*, 101–105, Brighton, U.K., Jun. 1979.
6. Abhik, G., K. Anirban, P. Manimala, and G. Rowdra, "A super wideband Chebyshev tapered antipodal Vivaldi antenna," *AEU Int. J. Electron. Commun.*, Vol. 69, 1328, 2015.

7. Furat, A. and F. Pascal, "A customized reduced size antipodal Vivaldi antenna used in wireless baseband transmission for short-range communication," *AEU Int. J. Electron. Commun.*, Vol. 70, 1684–1688, 2016.
8. Moosazadeh, M. and S. Kharkovsky, "A compact high-gain and front-to-back ratio elliptically tapered antipodal Vivaldi antenna with trapezoid-shaped dielectric lens," *IEEE Antennas Wirel. Propag. Lett.*, Vol. 15, 552–525, Mar. 2016.
9. Moosazadeh, M., S. Kharkovsky, and J. T. Case, "Microwave and millimetre wave antipodal Vivaldi antenna with trapezoid-shaped dielectric lens for imaging of construction materials," *IET Microwaves Antennas Propag.*, Vol. 10, No. 3, 301–309, 2016.
10. Wang, Z., J. Liu, and Y. Yin, "Triple band-notched UWB antenna using novel asymmetrical resonators," *AEU Int. J. Electron. Commun.*, Vol. 70, 1630–1637, 2016.
11. Li, W.-A., Z.-H. Tu, Q.-X. Chu, and X.-H. Wu, "Differential stepped-slot UWB antenna with common-mode suppression and dual sharp-selectivity notched bands," *IEEE Antennas Wireless Propag. Lett.*, Vol. 15, 1120–1123, 2016.
12. Chu, Q.-X., C.-X. Mao, and H. Zhu, "A compact notched band UWB slot antenna with sharp selectivity and controllable bandwidth," *IEEE Trans. Antennas Propag.*, Vol. 61, No. 8, 3961–3966, Aug. 2013.
13. Reddy, K. A., S. Natarajamani, and S. K. Behera, "Antipodal Vivaldi antenna UWB antenna with 5.5 GHz band-notch characteristics," *Proc.Int. Conf. Comput., Electron. Elect. Technol.*, 821–824, Kumaracoil, India, 2012.
14. Ye, L.-H. and Q.-X. Chu, "Improved band notched UWB slot antenna," *Electron. Lett.*, Vol. 45, No. 25, 1890–1897, Dec. 2009.
15. Choi, H.-S., T.-W. Kim, H.-Y. Hwang, and K. Choi, "An UWB antenna design with adjustable second rejection band using a SIR," *IEEE Trans. Magn.*, Vol. 50, No. 2, 913–916, Feb. 2014.
16. Siddiqui, J. Y., C. Saha, and Y. M. M. Antar, "Compact SRR loaded UWB circular monopole antenna with frequency notch characteristics," *IEEE Trans. Antennas Propag.*, Vol. 62, No. 8, 4015–4020, Aug. 2014.
17. Yang, D., S. Liu, M. Chen, and Y. Wen, "A compact Vivaldi antenna with triple band-notched characteristics," *Proc. IEEE 6th Int. Symp. Microw., Antenna, Propag., EMC Technol.*, 216–219, Shanghai, China, 2015.
18. Sarkar, D. and K. V. Srivastava, "SRR-loaded antipodal Vivaldi antenna for UWB applications with tunable notch function," *Proc. Int. Symp. Electromagn. Theory*, 466–469, Hiroshima, Japan, 2013.
19. John, M., M. J. Ammann, and P. McEvoy, "UWB vivaldi antenna based on a spline geometry with frequency band-notch," *Proc. IEEE Int. Symp. Antennas Propag. Soc. (AP-S)*, 1–4, Jul. 5–11, 2008.
20. Aravinda Reddy, K., S. Natarajamani, and S. K. Behera, "Antipodal Vivaldi antenna UWB antenna with 5.5 GHz band-notch characteristics," *International Conference on Computing, Electronics and Electrical Technologies (ICCEET)*, 821–824, Kumaracoil, 2012.
21. Yao, L., J. Xiao, H. Zhu, N. Li, and X. Li., "A high gain UWB Vivaldi antenna with band notched using Capacitively Loaded Loop (CLL) resonators," *IEEE International Conference on Microwave and Millimeter Wave Technology (ICMMT)*, 820–822, Beijing, 2016.
22. Yang, D., S. Liu, M. Chen, and Y. Wen, "A compact Vivaldi antenna with triple band-notched characteristics," *IEEE 6th International Symposium on Microwave, Antenna, Propagation, and EMC Technologies (MAPE)*, 216–219, Shanghai, 2015.
23. Zhang, B., K. Zhang, S. Yang, and H. Zhai, "A Vivaldi antenna with adjustable in-band notched characteristic," *Asia Pacific International Symposium on Electromagnetic Compatibility (APEMC)*, 713–715, Shenzhen, 2016.
24. Constantine, A., *Balanis Antenna Theory: Analysis and Design*, 1072, 3rd Edition, John Wiley & Sons, Inc., Hoboken, New Jersey, 2005.

25. Alshamaileh, K. A., M. J. Almalkawi, and V. K. Devabhaktuni, "Dual band-notched microstrip-fed Vivaldi antenna utilizing compact EBG structures," *International Journal of Antennas and Propagation*, Vol. 2, 1–7, 2015.
26. Abubakar, S. A., T. H. Masri, W. A. W. Z. Abidin, K. H. Ping, and H. T. Su, "Corrugated band-notched antipodal Vivaldi antenna using mushroom type EBG structure for wideband applications,"
27. Elsheakh, D. M. and E. A. Abdallah, "Ultrawideband Vivaldi antenna for DVB-T, WLAN, and WiMAX applications," *International Journal of Antennas and Propagation*, 2014.
28. Tang, T. and K. Lin, "An ultrawideband MIMO antenna with dual band-notched function," *IEEE Antennas Wireless Propag. Lett.*, Vol. 13, 1076–1079, 2014.
29. Kang, L., H. Li, X. Wang, and X. Shi, "Compact offset microstrip-fed MIMO antenna for band-notched UWB applications," *IEEE Antennas Wireless Propag. Lett.*, Vol. 14, 1754–1757, 2015.
30. Zhao, H., F.-S. Zhang, and X.-K. Zhang, "A compact band-notched Ultra-wideband spatial diversity antenna," *Progress In Electromagnetics Research C*, Vol. 51, 19–26, 2014.
31. Gao, P., S. He, and X. Wei, "Compact printed UWB diversity slot antenna with 5.5-GHz band-notched characteristics," *IEEE Antennas Wireless Propag. Lett.*, Vol. 13, 376–379, 2014.
32. Liu, L., S. W. Cheung, and T. I. Yuk, "Compact MIMO antenna for portable UWB applications with band-notched characteristic," *IEEE Trans. Antennas and Propag.*, Vol. 63, No. 5, 1917–1924, May 2015.
33. Li, D. H., F. S. Zhang, L. X. Cao, and Y. Zhao. "A compact dual band-rejected MIMO Vivaldi antenna for UWB wireless applications," *Progress In Electromagnetics Research Letters*, Vol. 86, 97–105, 2019.
34. Sultan, K. S. and H. H. Abdullah, "Planar UWB MIMO-diversity antenna with dual notch characteristics," *Progress In electromagnetics Research C*, Vol. 93, 119–129, 2019.
35. Sultan, K. S., O. M. A. Dardeer, and H. A. Mohamed, "Design of compact dual notched self-complementary UWB antenna," *Open Journal of Antennas and Propagation*, Vol. 5, No. 3, 99–109, 2017.